Crystal structure and phase transition of 4-aminopyridinium tetrachlorobismuthate(III), [4-$NH_2C_5H_4NH$][$BiCl_4$], as studied by x-ray diffraction, dielectric, proton NMR and infrared spectroscopy

2006 J. Phys.: Condens. Matter 18 5087

(http://iopscience.iop.org/0953-8984/18/22/009)

INSTITUTE OF PHYSICS PUBLISHING JOURNAL OF PHYSICS: CONDENSED MATTER

J. Phys.: Condens. Matter **18** (2006) 5087–5104 doi:10.1088/0953-8984/18/22/009

Crystal structure and phase transition of 4-aminopyridinium tetrachlorobismuthate(III), [4-$NH_2C_5H_4NH$][$BiCl_4$], as studied by x-ray diffraction, dielectric, proton NMR and infrared spectroscopy

B Kulicka[1], V Kinzhybalo[1,2], R Jakubas[1], Z Ciunik[1], J Baran[2] and W Medycki[3]

[1] Faculty of Chemistry, University of Wrocław, Joliot—Curie 14, 50–383 Wrocław, Poland
[2] Institute of Low Temperature and Structure Research, PAS, Okólna 2, 50-950 Wrocław, Poland
[3] Institute of Molecular Physics, PAS, Smoluchowskiego 17, 60-179 Poznań, Poland

Received 22 December 2005, in final form 14 March 2006
Published 19 May 2006
Online at stacks.iop.org/JPhysCM/18/5087

Abstract

The crystal structure of 4-aminopyridinium tetrachlorobismuthate(III), [4-NH_2PyH][$BiCl_4$], has been determined at 100 and 260 K by the x-ray diffraction method as monoclinic space group, $P2_1/c$ and $C2/c$, respectively. Differential scanning calorimetry and dilatometry reveal one perfectly reversible discontinuous phase transition at 254/255 K (cooling/heating) with $\Delta S = 10.1$ J mol^{-1} K^{-1}. The ^{1}H NMR spin–lattice relaxation time (T_1) and second moment (M_2) measurements disclose a significant change in the motional state of the cations near the phase transition temperature. Infrared spectra of polycrystalline [4-NH_2PyH][$BiCl_4$] have been studied in the temperature range 10–306 K. Substantial changes in the temperature evolution of frequencies of internal modes of the 4-aminopyridinium cations near 255 K are due to the change in the dynamics of cationic moieties. The experimental results indicate that the motion of the organic cations contributes mainly to the mechanism of an 'order–disorder' transition in [4-NH_2PyH][$BiCl_4$].

(Some figures in this article are in colour only in the electronic version)

1. Introduction

The molecular–ionic halogenoantimonates(III) and halogenobismuthates(III) of the general formula $R_aM_bX_{3b+a}$ (where M = Sb, Bi and X = Cl, Br, I) that contain in their structure organic cations evoke considerable interest because of their ferroic properties [1–5]. Salts with the $R_3M_2X_9$ or $R_5M_2X_{11}$ composition deserve special attention since they exhibit ferroelectric properties. In the former subclass, polar properties are encountered in ionic salts containing

the $CH_3NH_3^+$ [6], $(CH_3)_2NH_2^+$ [7, 8] or $(CH_3)_3NH^+$ [9, 10] cations. In the case of the $R_5M_2X_{11}$ subclass four salts containing cations of different sizes, methylammonium [11, 12], pyridinium [13] or imidazolium [14], are known. All salts that possess this composition appeared to have the ferroelectric properties. The paraelectric–ferroelectric phase transitions found in $R_5Bi_2X_{11}$ and $R_3M_2X_9$ subgroups were classified as 'order–disorder' type. The origin of the ferroelectricity is evidently due to the dynamics of dipolar organic cations.

4-Aminopyridinium tetrachloroantimonate(III), $[4\text{-}NH_2C_5H_4NH][SbCl_4]$ (4-APCA), is the first known example of a ferroelectric from the $R_aM_bX_{3b+a}$ family characterized by the $RSbX_4$ composition. 4-APCA was found to undergo the following complex sequence of phase transitions [15]:

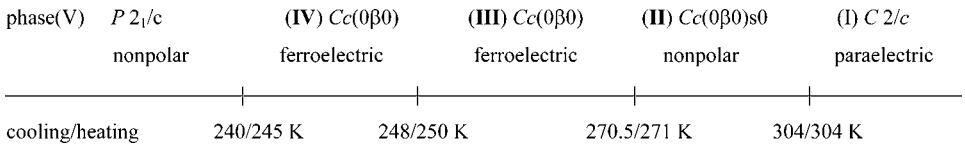

The phase **II** appears to be incommensurately modulated, whereas the lower temperature ones **III** and **IV** are commensurately modulated along the *b*-axis. The crystal is a ferroelectric below 270.5 K with relatively small spontaneous polarization of the order of 3.5×10^{-3} C m^{-2} placed within the *ac* plane. It is interesting that the ferroelectric properties of 4-APCA extend over phases **III** and **IV** and disappear below 240 K. The ferroelectric transition at 270.5 K is accompanied by a distinct dielectric anomaly ($\varepsilon_{max}(T_c) \approx 700$). The ferroelectric phase transition mechanism was suggested to be related to the dynamics of the 4-aminopyridinium cations. Nevertheless, AC calorimetric specific-heat measurements have shown that the incommensurate ferroelectric transition has both 'order–disorder' and 'displacive' contributions [16]. In the incommensurate phase **II** the apparent critical slowing down of the dielectric relaxation process is found with $\tau \approx 1 \times 10^{-4}$ s just above $T_c = 270$ K [17]. We decided to study a bismuth analogue, 4-aminopyridinium tetrachlorobismuthate(III)–$[4\text{-}NH_2PyH][BiCl_4]$, to find out how the replacement of the Sb atoms by the Bi ones modifies the structural and physical properties of the crystal. In this paper we report the crystal structures of the high and low temperature phases, and the differential scanning calorimetry (DSC), dilatometry, dielectric, proton magnetic resonance (^{1}H NMR) and infrared studies on $[4\text{-}NH_2PyH][BiCl_4]$. The mechanism of the structural phase transition at 255 K is proposed.

2. Experimental details

The starting materials were commercial $(BiO)_2CO_3$ and 4-aminopyridine. The (4-aminopyridinium) tetrachlorobismuthate(III) ($(4\text{-}NH_2PyH)BiCl_4$) crystals were prepared by dissolving stoichiometric amounts of $(BiO)_2CO_3$ and 4-aminopyridine in concentrated HCl solution. Single crystals of $[4\text{-}NH_2PyH][BiCl_4]$ were grown from an aqueous solution that contained hydrochloric acid to prevent the hydrolysis of $BiCl_3$.

The complex electric permittivity $\varepsilon^* = \varepsilon' - i\varepsilon''$ between 100 and 400 K was measured with HP 4285A precision *LCR* meters in the frequency range between 75 kHz and 30 MHz. The dimensions of the sample were approximately $5 \times 5 \times 1$ mm^3. The overall error was less than 5% for the real and imaginary parts of the complex electric permittivity.

Differential scanning calorimetry (DSC) was recorded using a Perkin Elmer DSC-7 in the temperature range 100–450 K. Thermogravimetric analysis (TGA) and differential thermal analysis (DTA) measurements were performed on a Setaram SETSYS 16/18 instrument in the temperature range 300–450 K.

Infrared spectra of the powdered [4-NH_2PyH][$BiCl_4$] sample in Nujol (KBr windows) and in the temperature range 10–306 K were recorded with a Bruker IFS-88 spectrometer with a resolution of 0.5 cm^{-1}. The Displex model CS-202 refrigeration system of APD Cryogenics Inc equipped with the Scientific Instruments Inc. temperature controller (Series 5500) was used for the low temperature measurements. The Galactic Industries program GRAMS/386 was used for numeral fitting of the experimental data.

The T_1 relaxation time measurements were performed on a Bruker SXP 4-100 spectrometer working at the frequency of 90 MHz. The temperature of the sample was automatically stabilized by the standard Bruker liquid nitrogen system (90 MHz). The T_1 relaxation times were determined by using the saturation method. The powdered sample of the crystal was degassed under pressure of 10^{-5} Torr and sealed under vacuum in glass ampoules. The second moment of NMR lines for protons was determined by analysis of the solid echo shape.

The x-ray diffraction data were collected on an automatic x-ray four-circle Excalibur PX diffractometer with CCD area detector at 100 and 260 K. Graphite monochromated Mo Kα radiation was generated at 50 kV and 25 mA. ϕ- and ω-scans were used to collect intensities of the reflections. The lattice parameters were calculated at all reflection positions. For measurement at both temperatures an Oxford cryo-system was used. Data collection and reduction were made using crysAlis CCD and crysAlis RED [18].

The crystal structures were solved by the direct method (SHELXS program [19]). The C- and N-bound H atoms for the low temperature structure were refined using a riding model, with C–H and N–H distances equal to 0.95 and 0.88 Å, respectively, and $U_{iso}(H) = 1.2U_{eq}$ (C or N).

Measurements of the cell parameters *versus* temperature were made with a Kuma KM4 four-circle diffractometer with single-point detector in the temperature range 120–285 K by refinement of 34 reflection positions.

Crystallographic data for the structures reported in this paper (excluding structure factors) have been deposited with the Cambridge Crystallographic Data Centre, CCDC no 293582 and 293583. Copies of this information may be obtained free of charge from the Director, CCDC, 12 Union Road, Cambridge CB2 1EZ, UK (fax, +44-1223-336033; e-mail, deposit@ccdc.cam.ac.uk or http://www.ccdc.cam.ac.uk).

3. Results

3.1. Thermal studies

3.1.1. Differential scanning calorimetry (DSC). The DSC curves for the [4-NH_2PyH][$BiCl_4$] crystals recorded upon heating (scans 2 and 4) and cooling (scans 1 and 3) at two different rates (30 and 5 K min^{-1}) are displayed in figure 1(a). The calorimetric measurements show that the crystal studied undergoes fully reversible discontinuous phase transition at 254/255 K (on cooling–heating, respectively). The transition entropy determined from the peak area is equal to 10.1 ± 1 J mol^{-1} K^{-1}. Taking into account the transition entropy value the phase transition may be classified as 'order–disorder'. It should be added that the observed peak at lower scanning rate (5 K min^{-1}) is asymmetric with a clear shoulder from the lower temperature side. One can suggest that the mechanism of phase transition is complex and it is expected to proceed by two steps.

3.1.2. Dilatometry. The temperature dependence of the linear thermal expansion was performed along two various directions (the *b*-axis and one direction perpendicular to the *b*-axis) in the close vicinity of the expected phase transition to confirm the phase situation

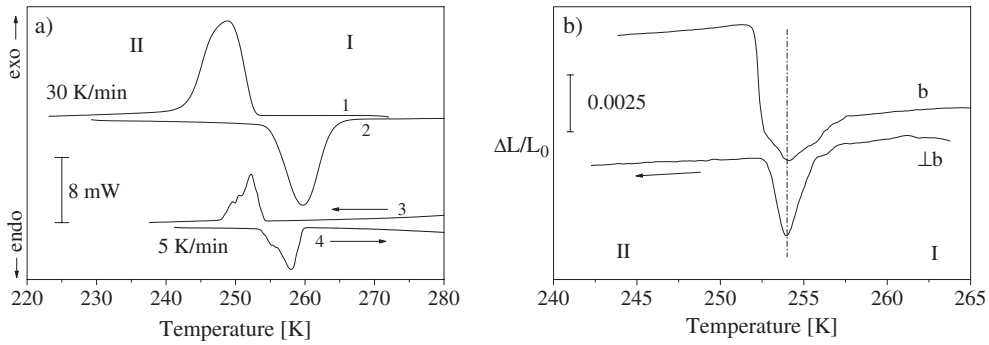

Figure 1. (a) DSC curves obtained on heating and cooling at various rates (30 and 5 K min^{-1}); sample mass, 23.2 mg; (b) temperature dependence of the linear thermal expansion $\Delta l/L_o$ along the b and $\perp b$ directions.

disclosed by the calorimetric measurements. The dilatometric measurements, in contrast to the x-ray ones, better reflect the qualitative changes in a narrow temperature range. The best dilatometric characteristics were obtained during the cooling scans. The dilation of [4-NH_2PyH][$BiCl_4$] is shown in figure 1(b). Along the b-axis close to 257 K a visible change in the slope of the linear part of the dilation takes place, whereas a rapid expansion of the sample is observed approaching 254 K. For the second direction ($\perp b$) both a dilation and expansion of the sample for the corresponding temperature region is observed. This result seems to be consistent with the calorimetric one, suggesting a rather complex mechanism of the structural phase transition.

3.2. The dielectric results

The dielectric measurements were made for the electric field parallel along the b-axis. We were able to perform the measurements only along this axis since it is perpendicular to the natural large plane of the single crystal. The crystals are too fragile to cut out and polish samples to prepare other directions.

The phase transition at 254 K (first cooling scan) is accompanied by breakage of a single crystal sample, which produces large numbers of defects, falsifying the real dielectric response. Figure 2 shows the temperature dependence of the permittivity, ε'_b, below room temperature in the frequency range 500 kHz and 20 MHz upon the second cooling scan. The phase transition at 254 K is accompanied by a rapid drop of the permittivity by about two units. The dielectric response may be explained in terms of a sudden 'freeze-out' of orientational motion of dipolar organic units. No dielectric relaxation process is disclosed both over phase **I** and **II**. This means that the motion of dipolar groups above $T_{c(I\rightarrow II)}$ is rather fast and the expected macroscopic relaxation time is shorter than 1×10^{-8} s.

3.3. The x-ray measurements

The crystal structure of [4-NH_2PyH][$BiCl_4$] was determined at 100 and 260 K to verify the phase situation disclosed by the above mentioned experimental methods. Both phases (**II** and **I**—the phases below and above the 254/255 K transition point, respectively) appear in the monoclinic space group. Crystallographic data and details on the structure determinations at two temperatures are given in table 1. The independent parts of the title crystal at two temperatures are illustrated in figures 3(a) and (b). The crystal structure is built up of infinite

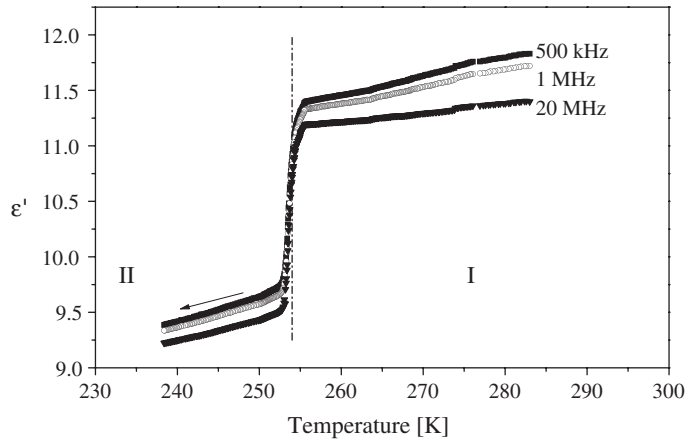

Figure 2. Temperature dependence of the real part of the complex electric permittivity, ε', measured along the *b*-axis at frequencies between 500 kHz and 20 MHz upon cooling.

Table 1. Crystal data and structure refinement for [4-NH_2PyH][$BiCl_4$].

Phase	**II**	**I**
Empirical formula	[4-NH_2PyH][$BiCl_4$]	[4-NH_2PyH][$BiCl_4$]
Formula weight	445.91	445.91
Temperature	100(2) K	260(2) K
Wavelength	0.710 73 Å	0.710 73 Å
Crystal system	Monoclinic	Monoclinic
Space group	$P2_1/c$	$C2/c$
Unit cell dimensions	$a = 11.175(2)$ Å	$a = 13.220(2)$ Å
	$b = 13.595(2)$ Å	$b = 13.498(2)$ Å
	$c = 7.275(1)$ Å	$c = 7.326(1)$ Å
	$\beta = 93.74(1)$ Å	$\beta = 120.51(1)$ Å
Volume	1102.9(3) $Å^3$	1126.2(3) $Å^3$
Z	4	4
Calculated density	2.692 Mg m^{-3}	2.630 Mg m^{-3}
Absorption coefficient	16.906 mm^{-1}	16.556 mm^{-1}
$F(000)$	808	808
Crystal size	0.15 × 0.09 × 0.05 mm^3	0.12 × 0.09 × 0.06 mm^3
Theta range for data collection	3.18°–27°	4.87°–27°
Ranges of h, k, l	$-14 \leqslant h \leqslant 13 - 16$	$-13 \leqslant h \leqslant 16 - 17$
	$\leqslant k \leqslant 17 - 8 \leqslant l \leqslant 9$	$\leqslant k \leqslant 17 - 9 \leqslant l \leqslant 7$
Reflections collected	11 716	4894
Independent reflections R_{int}	2420(0.0769)	1091(0.1508)
Data/restraints/parameters	2420/0/109	1091/60/76
Goodness of fit on F^2	1.042	1.388
Final R_1/wR_2 indices	0.0228/0.0576	0.0569/0.1733
Largest diff. peak/hole	1.351/−0.965	2.833/−2.566

chains $[BiCl_4^-]_\infty$. They extend along the *c*-direction (see figures 4(a) and (b)). The inorganic chains consist of edge-sharing $BiCl_6$ octahedrons. The 4-aminopyridinium cations are π-stacked along the *c*-axis. In the **II** phase all 4-aminopyridinium moieties are completely ordered. The Bi–Cl distances fall into three ranges: ∼2.5 Å—two terminal Cl atoms (Cl3 and

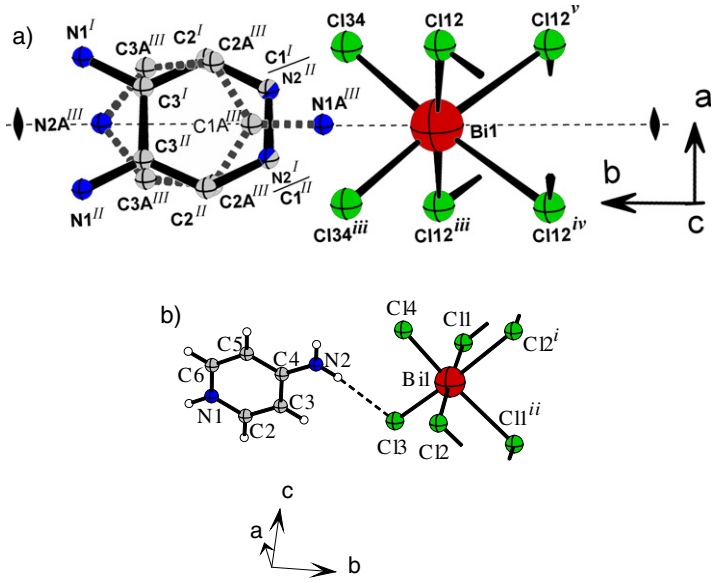

Figure 3. (a) The numbering scheme of the [4-NH_2PyH][$BiCl_4$] crystal in the high temperature phase (**I**) at 260 K. Three possible positions of the 4-aminopyridinium cations are presented: positions I and II are related to each other by a twofold axis, represented by a broken line passing through the N1A, N2A, C1A and Bi1 atoms; (b) the numbering scheme of the asymmetric unit of the [4-NH_2PyH][$BiCl_4$] crystal in the low temperature phase (**II**) at 100 K.

Cl4), ∼2.7 and ∼3.0 Å—two pairs of bridging Cl atoms (Cl1, Cl2 and $Cl1^{ii}$, $Cl2^{i}$ respectively) (see table 2). The N–H ··· Cl hydrogen bonds (∼3.3–3.4 Å donor–acceptor distance) are classified as a weak ones (see table 3); nevertheless, they may slightly distort the inorganic fragment of the crystal.

The space group changes from $C2/c$ to $P2_1/c$ during the phase transition at 254 K (upon cooling). Nevertheless, this transition (**I** → **II**) is not classified as a 'nonferroic' phase transition, because it is not accompanied by a multiplication of the crystal's unit cell [20]. The 4-aminopyridinium cations occupy the sites of C_2 symmetry, which implies their orientational disorder. Considering a strong thermal motion of the 4-aminopyridinium moieties it was rather difficult to recognize their definite positions. Two symmetrically equivalent positions assigned as I and II correspond to that found in **II** (see figure 3(b)). High difference Fourier peaks and incomplete occupation of positions I and II forced us to look for an alternative location for the organic cation. A careful analysis of the difference Fourier map enabled recognition of position III. However, it should be added that the reorientation of the 4-aminopyridinium moieties between two sites, from I or II to III, in such a strained environment seems to be rather difficult, that is justified by a low occupation of position III.

Upon cooling, the inorganic fragment undergoes a slight distortion. Due to higher symmetry of **I** there are only two crystallographically independent halogen atoms in this phase, namely Cl12 and Cl34, which correspond to the Cl1, Cl2 and Cl3, Cl4 atom positions, respectively, in **II**. These deformations result in a volume decrease of cavities occupied by the 4-aminopyridinium moieties, which limits the freedom of organic cation motion. Organic cation cavities are surrounded by eight halogen atoms, as shown in figure 5, that take part in H-bonds of N–H ··· Cl type and rather weak C–H ··· Cl interactions, and stabilize definite cation positions. Ordering of the 4-aminopyridinium moieties in phase **II** is responsible for

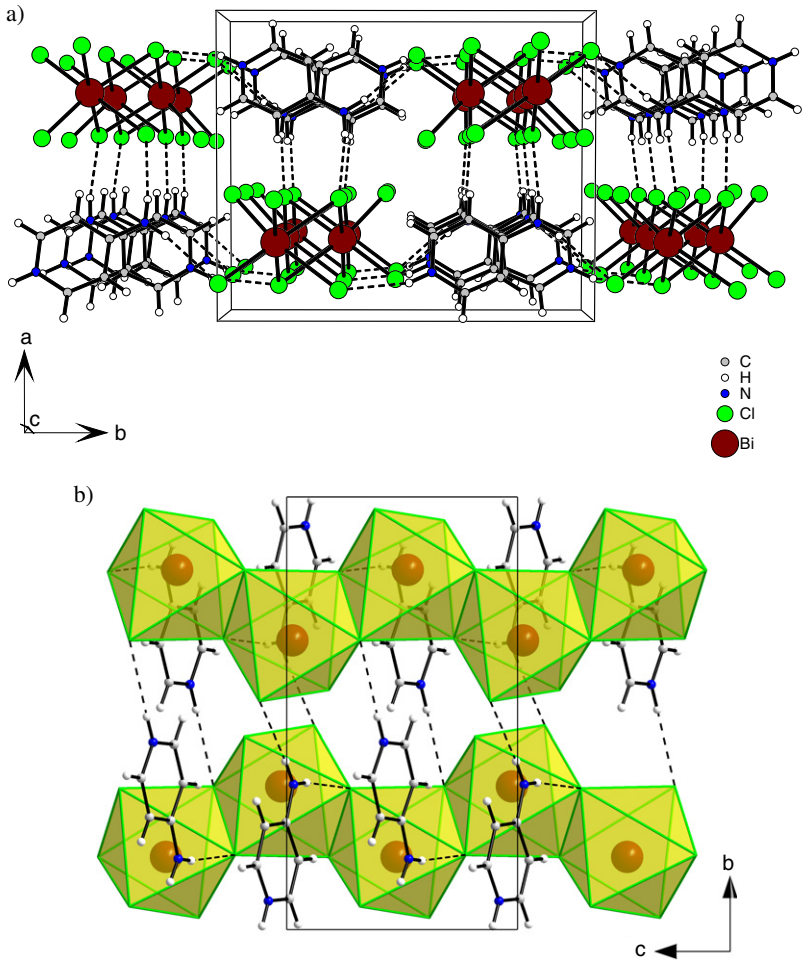

Figure 4. (a) Projection of the atomic arrangement along the *c*-axis in the low temperature phase (**II**) at 100 K; (b) projection of the atomic arrangement along the *a*-axis in the low temperature phase (**II**) at 100 K (the anions are shown in a polyhedral representation).

the inorganic fragment distortion. Let us compare, for example, two terminal chlorine atoms, namely Cl3 and Cl4 (**II**) and Cl34 (**I**). In phase **II**, the Cl3 atom takes part in the formation of the H-bond, whereas the Cl4 does not, which correlates well with the observed lengths of the Bi1–Cl3 and Bi1–Cl4 bonds: 2.5451(12) and 2.4901(11) Å, respectively.

On the basis of x-ray measurements one can state that in the high temperature phase (**I**) the cations reveal a dynamical disorder which is consistent with the calorimetric studies. Since the cations occupy the sites of C_2 symmetry, the change in arrangement of the cations has to lead to the lowering of the symmetry for the crystal at 255 K.

A smarter presentation of the thermal expansion of [4-NH_2PyH][$BiCl_4$] in comparison to that estimated by a linear thermal expansion method (TMA) results from the x-ray measurements. The temperature dependences of the lattice parameters, a, b and c, are illustrated in figure 6(a). The temperature variations of the monoclinic β angle and unit cell volume of [4-NH_2PyH][$BiCl_4$] are shown in figure 6(b). The most significant changes

Table 2. Selected bond lengths (Å) and angles (degrees) for [4-NH_2PyH][$BiCl_4$]. (Symmetry codes: (I) $x, 1/2 - y, 1/2 + z$; (II) $x, 1/2 - y, z - 1/2$; (III) $-x, y, 3/2 - z$; (IV) $-x, -y, 2 - z$; (V) $x, -y, z - 1/2$.)

Phase	**II**		**I**	
	Bi1 Cl4	2.4901(11)	Bi1 $Cl34^{III}$	2.513(4)
	Bi1 Cl3	2.5451(12)	Bi1 Cl34	2.513(4)
	Bi1 Cl2	2.7257(11)	Bi1 Cl12	2.730(5)
	Bi1 Cl1	2.7405(11)	Bi1 $Cl12^{III}$	2.730(5)
	Bi1 $Cl2^{I}$	2.9595(11)	Bi1 $Cl12^{IV}$	3.002(4)
	Bi1 $Cl1^{II}$	3.0612(12)	Bi1 $Cl12^{V}$	3.002(4)
	Cl4 Bi1 Cl3	92.60(4)	$Cl34^{III}$ Bi1 Cl34	92.6(3)
	Cl4 Bi1 Cl2	90.04(4)	$Cl34^{III}$ Bi1 Cl12	90.72(13)
	Cl3 Bi1 Cl2	90.47(4)	Cl34 Bi1 Cl12	90.61(15)
	Cl4 Bi1 Cl1	92.19(3)	$Cl34^{III}$ Bi1 $Cl12^{III}$	90.61(15)
	Cl3 Bi1 Cl1	89.36(4)	Cl34 Bi1 $Cl12^{III}$	90.72(13)
	Cl2 Bi1 Cl1	177.77(3)	Cl12 Bi1 $Cl12^{III}$	178.07(12)
	Cl4 Bi1 $Cl2^{I}$	85.92(4)	$Cl34^{III}$ Bi1 $Cl12^{IV}$	89.69(16)
	Cl3 Bi1 $Cl2^{I}$	174.27(3)	Cl34 Bi1 $Cl12^{IV}$	174.01(15)
	Cl2 Bi1 $Cl2^{I}$	95.06(3)	Cl12 Bi1 $Cl12^{IV}$	83.81(10)
	Cl1 Bi1 $Cl2^{I}$	85.18(3)	$Cl12^{III}$ Bi1 $Cl12^{IV}$	94.80(10)
	Cl4 Bi1 $Cl1^{II}$	169.81(3)	$Cl34^{III}$ Bi1 $Cl12^{V}$	174.01(15)
	Cl3 Bi1 $Cl1^{II}$	95.31(4)	Cl34 Bi1 $Cl12^{V}$	89.69(16)
	Cl2 Bi1 $Cl1^{II}$	83.48(3)	Cl12 Bi1 $Cl12^{V}$	94.80(10)
	Cl1 Bi1 $Cl1^{II}$	94.32(3)	$Cl12^{III}$ Bi1 $Cl12^{V}$	83.81(10)
	$Cl2^{I}$ Bi1 $Cl1^{II}$	86.82(3)	$Cl12^{IV}$ Bi1 $Cl12^{V}$	88.59(14)
	Bi1 Cl1 $Bi1^{I}$	94.34(3)	Bi1 Cl12 $Bi1^{IV}$	96.19(10)
	Bi1 Cl2 $Bi1^{II}$	96.99(3)	Bi1 $Cl12^{III}$ $Bi1^{III}$	96.19(10)

Table 3. Hydrogen bonds for [4-NH_2PyH][$BiCl_4$] (Å and degrees) at 100 K. (Symmetry codes: (I) $x, -y - 1/2, z - 1/2$; (II) $1 - x, -y, 1 - z$.)

D–H...A	d(D–H)	d(H...A)	d(D...A)	<DHA
N1–H1... $Cl1^{I}$	0.88	2.47	3.319(4)	161.3
N2–H2A... $Cl2^{II}$	0.88	2.60	3.467(5)	171.0
N2–H2B... Cl3	0.88	2.58	3.452(4)	170.3

are found along the b- and a-axes, with the expansion of about 0.9% and compression of about 1.35%, respectively. This large anomaly observed is ascribed to the structural phase transition ($T_{c(II\rightarrow I)}$). This transition is accompanied by an enormous change in the β-angle (nearly one degree), which justifies strong distortion of the lattice cell and breakage of a single crystal. The transition leads also to a positive change in the crystal volume by about 0.64%. The pressure coefficient for this first-order phase transition is estimated from the Clausius–Clapeyron relation:

$$dT_c/dp = \Delta V/\Delta S,$$

where $\Delta V/V = +6.4 \times 10^{-3}$ is the change in the molar volume and ΔS is the value of the transition entropy (10.1 J mol K). The pressure coefficient for the phase transition at 255 K (upon heating) is found to be about 0.1 K MPa^{-1}.

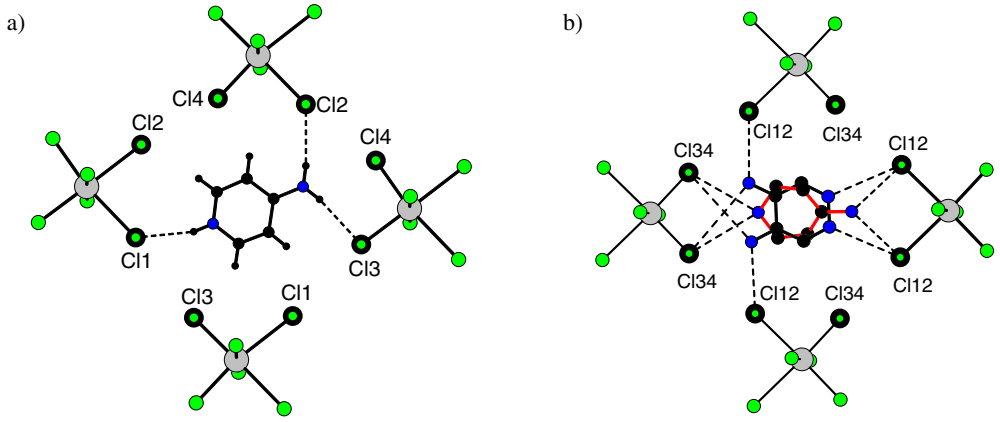

Figure 5. The hydrogen-bond configuration in the [4-NH_2PyH][$BiCl_4$] crystal along the *c*-axis (a) at 100 K and (b) at 260 K (H-bonds are represented by dashed lines).

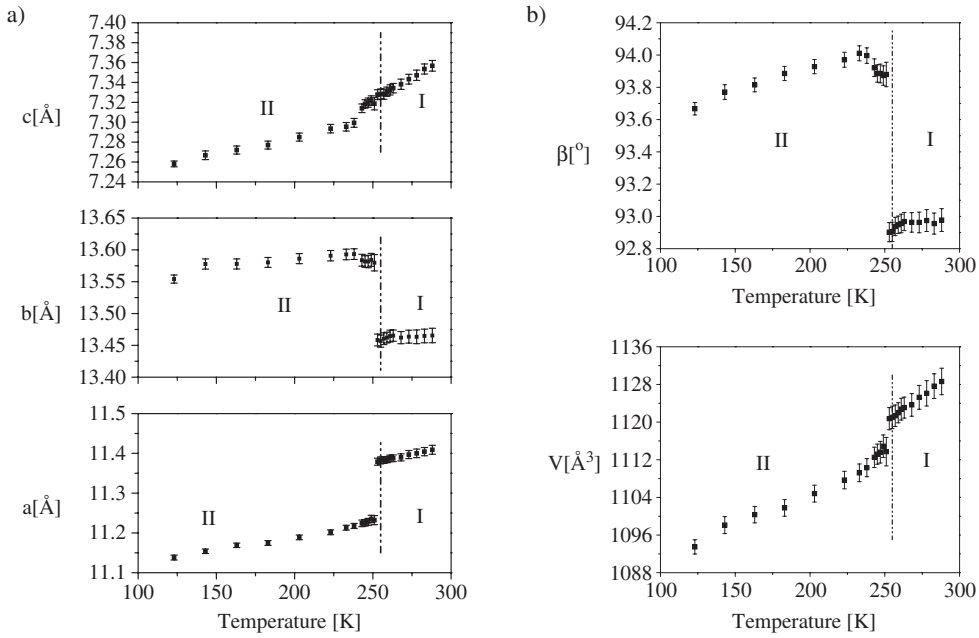

Figure 6. Experimental values of the lattice parameters *a*, *b* and *c* (a); the β monoclinic angle and volume of the unit cell (b), as a function of temperature for the [4-NH_2PyH][$BiCl_4$] crystal.

3.4. ^1H *proton magnetic resonance measurements*

The temperature dependence of the nuclear relaxation time T_1 for ^{1}H is shown in figure 7(b). The temperature dependence of the spin–lattice relaxation time measured does not reveal any fully shaped minimum. At the temperature of about 255 K the distinct discontinuity in $T_1(T)$ is visible. Both found slopes seem to be nearly symmetrical, but in fact from the low temperature slope the determined activation energy is equal to 15.5 kJ mol^{-1} and this energy is lower than the activation energy equal to 23.6 kJ mol^{-1} determined from the high temperature slope. It

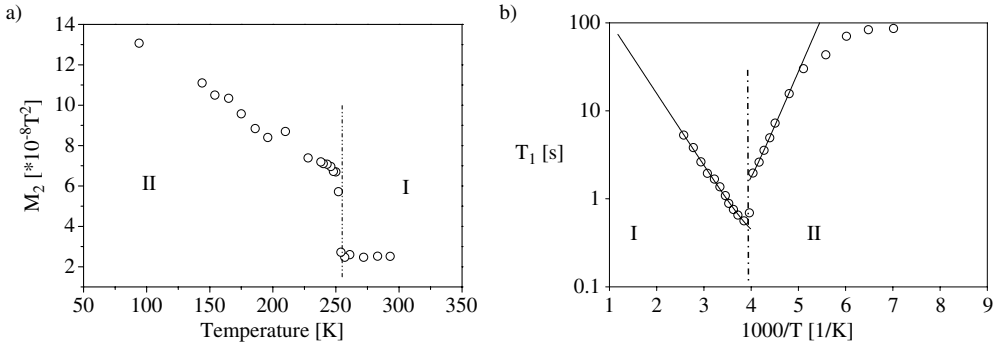

Figure 7. (a) Temperature dependence of the second moment (M_2) of the ^{1}H NMR line, (b) temperature dependence of the ^{1}H NMR spin–lattice relaxation time for [4-NH_2PyH][$BiCl_4$].

should be emphasized that a similar temperature characteristic of T_1 reveals a closely related compound containing the 4-aminopyridinium cations: [4-NH_2PyH][$SbBr_4$]. This compound also undergoes one structural phase transition at 222 K [21, 22]. Similarly as in the case of the bismuth analogue, the phase transition is accompanied by a significant jump in the T_1 value, while the minimum appears just before reaching the transition at 236 K. Unfortunately, in [4-NH_2PyH][$BiCl_4$] the expected minimum overlies with the anomaly on the $\log T_1(1/T)$ curve. It is interesting that nearly the same values of activation energies were found to appear for the corresponding phases of both analogues, e.g. in [4-NH_2PyH][$SbBr_4$], 12.2 kJ and 25.9 kJ mol^{-1} for the low and high temperature phases. This may suggest a similar motional behaviour of the cations over the corresponding phases for both isomorphous analogues.

The temperature changes in the second moment, M_2, of the ^{1}H NMR line are presented in figure 7(a). The M_2 value decreases monotonically from 13×10^{-8} T^2 at 90 K down to about 6×10^{-8} T^2 at the phase transition temperature, where an abrupt jump to 2.5×10^{-8} T^2 takes place. At temperatures above 255 K M_2 maintains a nearly constant value of about 2.5×10^{-8} T^2.

Molecular dynamics of the 4-aminopyridinium cation was studied by means of ^{1}H NMR in the ferroelectric [4-NH_2PyH][$SbCl_4$]. This crystal appeared to exist in the same space group ($P2_1/c$) in the low temperature ordered phase. This implies analogous dynamical properties of the organic cations. For the antimony analogue, in [23] the experimental and theoretical values of the second moment of the ^{1}H NMR signal were analysed and compared in detail. Based on these considerations one may propose possible types of motion for the cations in various phases of the [4-NH_2PyH][$BiCl_4$] crystal. The theoretical total second moment value (M_2) for the rigid structure was found to be 11.2×10^{-8} T^2. Within the experimental error the M_2 value in the bismuth analogue is quite close to that for the rigid structure, which indicates the full order of the cations at 100 K. Diminishing of the M_2 value approaching the transition temperature from 100 K may be explained in terms of an onset of a small-angle reorientation of the pyridinium ring. The plateau of M_2 observed over the room temperature phase (2.5×10^{-8} T^2) may be explained assuming an amplitude of about 60° for the 4-NH_2PyH^+ cation libration around their pseudo-sixfold axis. The theoretical M_2 value for such a type of motion was estimated to be 2.81×10^{-8} T^2, which is in excellent agreement with that found in our experiment. On the basis of the ^{1}H NMR one can conclude that a significant jump in the M_2 value at 255 K proves a drastic change in the motional state of the cations. These experimental results clearly indicate an important role of the 4-aminopyridinium cations in the molecular mechanism of the **II** $\rightarrow$ **I** phase transition.

Table 4. Formal classification of the fundamental modes ($k = 0$) for the [4-NH_2PyH][$BiCl_4$] crystal at low temperature phase **II**. (Abbreviations: i—inactive, T—translational, L—librational lattice modes.)

Low temperature (100 K) phase (**II**); Space group $P2_1/c = C_{2h}^5$; $Z = Z_B = 4$							
	External modes			Internal modes		Selection rules	
C_{2h}^5	Acoustic	T	L	4-ApyH$^+$	$BiCl_4^{1-}$	IR	Raman
A_g		6	6	36	9	i	xx, yy, zz, xz
B_g		6	6	36	9	i	xy, zy
A_u	1	5	6	36	9	Y	i
B_u	2	4	6	36	9	X, Z	i

Table 5. Formal classification of the fundamental modes ($k = 0$) for the [4-NH_2PyH][$BiCl_4$] crystal in high temperature phase **I**. (Abbreviations: i—inactive, T—translational, L—librational lattice modes.)

High temperature (260 K) phase **I**; space group $C2/c = C_{2h}^6$; $Z = 4$; $Z_B = 2$							
	External modes			Internal modes		Selection rules	
C_{2h}^6	Acoustic	T	L	4-ApyH$^+$	$BiCl_4^{1-}$	IR	Raman
A_g		2	2	17	5	i	xx, yy, zz, xz
B_g		4	4	19	4	i	xy, zy
A_u	1	1	2	17	5	Y	i
B_u	2	4	4	19	4	X, Z	i

3.5. Vibrational studies

The x-ray studies revealed that the dynamics of the organic cations in phase **II** (100 K) and in phase **I** (260 K) are drastically different. The cations are disordered in phase **I**. This disorder should be observed in the vibrational spectra as well.

Formal classification of the fundamental modes for the title crystal in the low and high temperature phases is given in tables 4 and 5, respectively. For the high temperature phase **I**, it is assumed that 4-aminopyridinium cations and $BiCl_4^-$ anions occupy the C_2 sites. Thus, the disorder observed for the 4-aminopyridinium cations by the x-ray methods was neglected. In this case, the internal modes of the 4-aminopyridinium cation can be classified as 17 A + 19 B according to the C_2 site symmetry. The internal vibrations of the $BiCl_4^-$ anions may be classified as 5 A + 4 B for phase **I**. Each A-type mode should split into two unit cell modes ($A_u + A_g$). Each B-type internal mode should also split into two unit cell modes ($B_g + B_u$). In the case of low temperature phase **II**, all ions occupy general C_1 sites. Therefore, each internal mode (A) should split into four ($A_g + B_g + A_u + B_u$) unit cell modes in phase **II**. As the unit (Bravais) cell contains twice as many symmetry equivalent ions for phase **II** ($Z_B = Z = 4$) as in the case of phase **I** ($Z_B = Z/2 = 2$), more bands are expected for phase **II** (45 A_u + 45 B_u modes in IR and 45 A_g + 45 B_g modes in Raman) than for phase **I** (22 A_u + 23 B_u in IR and 22 A_g + 23 B_g in Raman).

However, if the dynamical (Davydov) type interaction is neglected, one can expect a similar number of bands arising from the internal vibrations of 4-aminopyridinium cations (36) and from internal vibrations of $BiCl_4^-$ (nine) in both phases, respectively.

As follows from figure 8, great changes are observed between the IR spectra measured at 295 and 10 K. The observed wavenumbers of the bands and their assignment is given in table 6. The bands observed in the region 4000–400 cm^{-1} arise from the internal vibrations

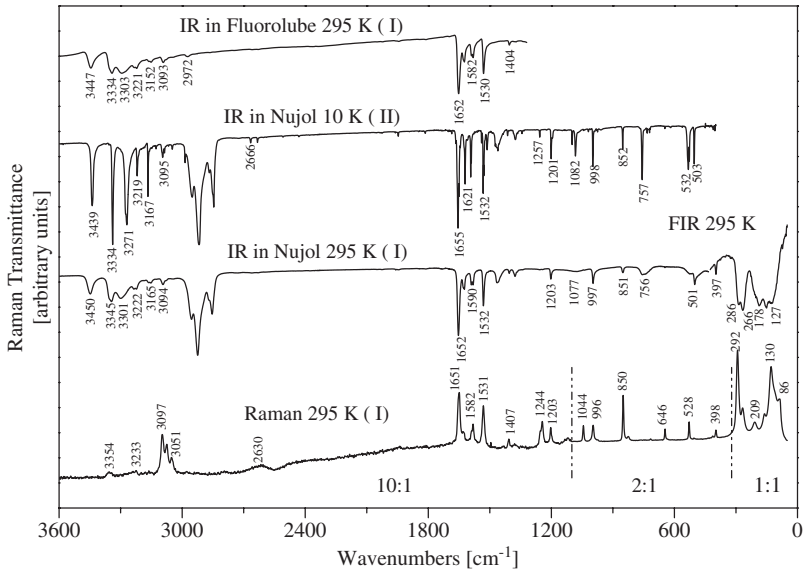

Figure 8. The FT-IR spectra measured at 10 and 295 K and FT-Raman spectrum measured at 295 K for the [4-NH_2PyH][$BiCl_4$] polycrystalline samples.

of the 4-aminopyridinium cations, and their assignment can be done taking into account other papers on vibrational spectra of 4-aminopyridine and its protonated salts [24–27]. The bands observed above 3100 cm^{-1} are due to the stretching vibrations of the NH_2 and NH^+ groups, which may be involved in the hydrogen bonds of rather weak strength. According to [24], the bands at 3450 and at about 3300 cm^{-1} may be due to the $\nu_a NH_2$ and $\nu_s NH_2$ vibrations. In such a case the band at about 3345 cm^{-1} should be assigned to the stretching vibration of the νNH^+, which is involved in a weak hydrogen bond.

Even in figure 9 one may notice some asymmetry of the 3450 cm^{-1} band, a clear shoulder at about 3358 cm^{-1} and a shoulder at 3270 cm^{-1}. On cooling down, the bands at 3439 and 3334 cm^{-1} become symmetrical. The band at 3271 cm^{-1} becomes very narrow and a clear shoulder is observed at 3277 cm^{-1}. These low temperature changes do not correspond to the selection rules shown in tables 4 and 5, which predict more bands at low temperature phase II than at phase I. This observation clearly shows that the selection rules discussed above are not obeyed, and that the observed changes are due to the change in the dynamical state of the organic cations. The temperature evolution of the region 3500–3000 cm^{-1} and the temperature changes of the wavenumbers of the bands and of the FWHM for the 3439 cm^{-1} band are shown in figure 9. The **I** → **II** phase transition affects all bands observed. It is characteristic that most of the bands exhibit splitting in phase **I**, which disappears in phase **II**. The 3300 cm^{-1} band shows a significant shift down by nearly 30 cm^{-1} at 250 K. On going from **II** to **I** phase the FWHM of the 3439 cm^{-1} mode reveals an important increase of almost 12 cm^{-1}.

Similar changes across the phase transition at 250 K are observed for the bands appearing in between 1500 and 1700 cm^{-1} (figure 10). Again it is quite surprising that the modes at about 1620 and 1590 cm^{-1} split into two components on going from the low to high temperature phase.

The temperature evolution of the spectra in the regions of 925 and 730 cm^{-1} is displayed in figure 11. Particularly great changes are observed for the 758 cm^{-1} band. This band

Table 6. Wavenumber, intensity and tentative assignments of the bands observed in the IR spectra in [4-NH_2PyH][$BiCl_4$] at 10 and 295 K and Raman at 295 K. (sh—shoulder, vs—very strong, s—strong, m—medium, w—weak, vw—very weak.)

IR		Raman		IR		Raman	
10 K	295 K	295 K	Assignment	10 K	295 K	295 K	Assignment
3439 s	3450 w	3354 vw	$\upsilon_a(NH_2)$	1608 vw		1591 vw	8a
	3358 m sh		$\nu(NH^+)$	1602 vw			
3334 vs	3345 m			1593 m	1590 w		
3277 s sh	3301 w		$\upsilon_s(NH_2)$	1590 w			
3271 vs					1582 w	1582 vw	ν_{ring}
3252 sh vw				1540 vw			
	3234 w	3233 vw		1532 m	1532 m	1531 vw	
3219 w	3222 w			1529 m	1529 sh vw		
3214 vw				1523 vw			
3167 m	3165 vw		$\nu_{C=C}$	1513 vw			19a
3150 vw	3152 vw				1404 w[a]	1407 vw	
3127 vw					1380 vw[a]		
3095 vw	3094 vw	3097 vw			1372 vw[a]		
3086 vw	3077 vw	3075 vw	ν(CH)	1334 vw			
3048 vw		3051 vw		1257 vw		1255 vw	ν(C-NH_2)
	2973 vw[a]					1244 vw	
	2939 vw[a]			1201 w	1203 vw	1203 vw	
	2864 vw[a]			1195 vw	1197 sh vw		
	2841 vw[a]			1099 vw			δNH^+
	2745 vw[a]			1082 vw	1077 vw		
2666 vw	2667 vw			1042 vw		1044 vw	δ_{ring}
2633 vw	2627 vw	2630 vw		1020 vw			
2604 vw				1009 vw			
2598 vw				998 w	997 w	996 vw	Ring breath.
2589 vw				989 vw			
2508 vw				978 vw			
2500 vw				975 vw		975 vw	
2452 vw				852 w	851 vw	850 w	$11-\gamma(CH)$
2431 vw	2419 vw					825 vw	
2378 vw	2375 vw			769 vw			
2055 vw	2050 vw			757 m	756 vw		γNH^+
2052 vw				647 vw	646 vw	646 vw	δ_{ring}
2036 vw				562 vw			
2031 vw	2029 vw			535 vw			
2025 vw	2023 vw			532 m			ρNH_2
1961 vw	1958 vw			527 w	526 vw sh	528 vw	
1946 vw	1945 vw			503 w	501 w		
1893 vw	1893 vw				397 vw	398 vw	γ_{ring}
1847 vw					286 m	292 vs	ν BiCl terminal
1815 vw	1812 vw				266 m	266 w	
1686 vw						209 w	ν BiCl bridge
1666 vw					187 m		
1660 sh m					151 m	162 w	
1655 vs	1652 vs	1651 vw	$\delta(NH_2)$		127 m	130 vs	
1650 s sh						115 sh m	Bending modes
1644 vw						86 m	
	1630 w	1630 vw			73 vw		Lattice mode
1626 vw			$\nu^+_{C=N}$ and $\delta(NH^+)$		56 vw		
1621 m	1624 w						
1612 vw							

[a] In Fluorolube.

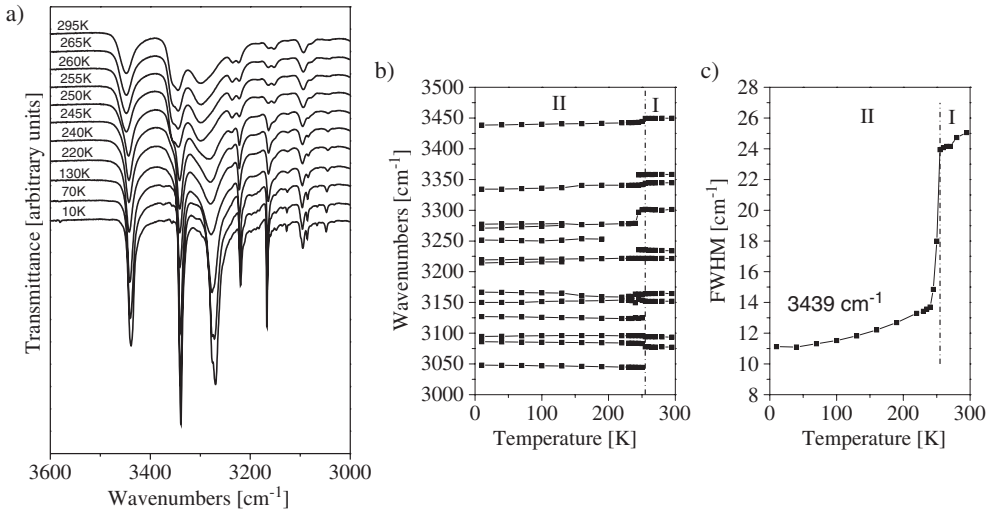

Figure 9. (a) The evolution of the infrared spectra of [4-NH_2PyH][$BiCl_4$] at several temperatures of the stretching modes, NH_2, and (C–H), in the frequency region 3600–3000 cm^{-1}; (b) temperature dependence of the bands in this wavenumber range; (c) temperature dependence of FWHM for the 3439 cm^{-1} modes.

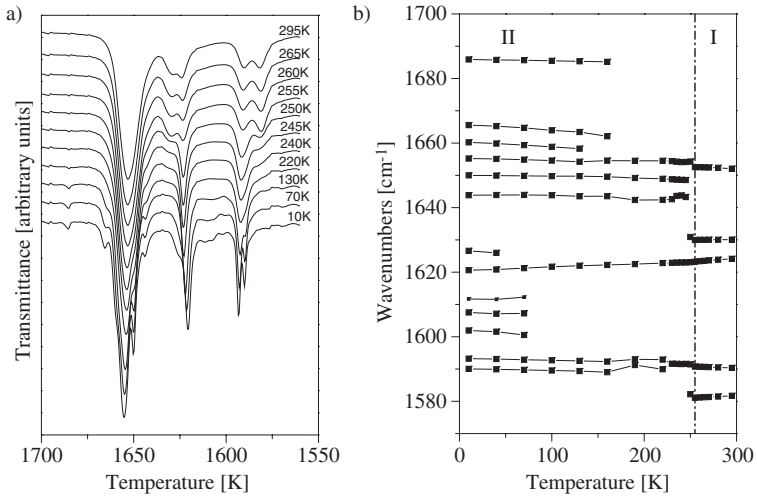

Figure 10. (a) The temperature evolution of the powder infrared spectra and (b) variations of the band positions with temperature in the frequency region 1700–1550 cm^{-1} for the [4-NH_2PyH][$BiCl_4$] crystal.

may arise from the out-of-plane bending mode of $NH^+ \cdots Cl$ hydrogen bonds. The in-plane bending mode of these hydrogen bonds may be observed at about 1082 cm^{-1}. Particularly great changes are also observed for the band at about 526 cm^{-1}, which may be due to the twisting (or librational) modes of the NH_2 group (see figure 12). All these observations confirm that the 4-aminopyridinium cations experience a dramatic change in motional state on the phase transition and that the cationic sublattice plays a major role in the molecular mechanism of the

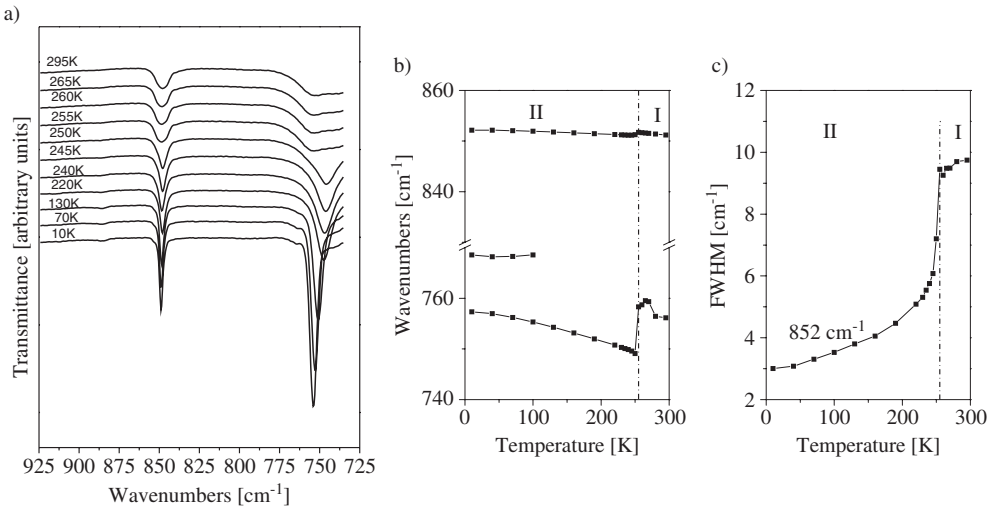

Figure 11. (a) The temperature evolution of the powder infrared spectra and (b) variations of the band positions with temperature in the frequency region 740–860 cm^{-1} and also (c) the temperature dependence of the bandwidth (FWHM) of the 852 cm^{-1} mode for the [4-NH_2PyH][$BiCl_4$] crystal.

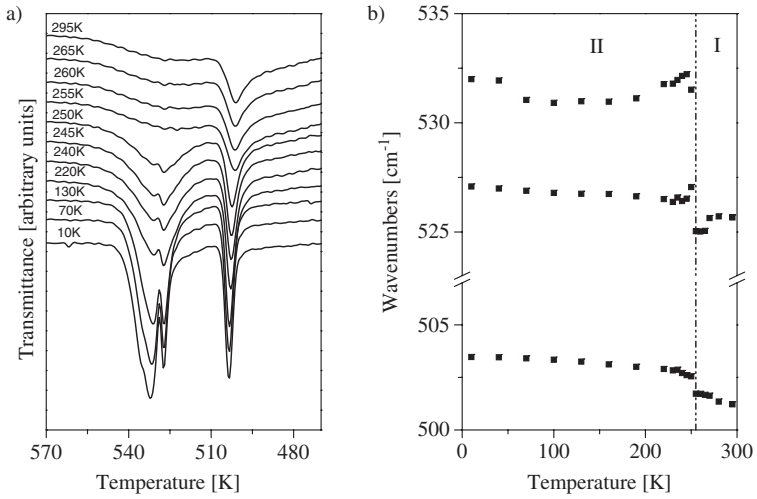

Figure 12. (a) The temperature evolution of the powder infrared spectra and (b) variations of the band positions with temperature in the frequency region 480–570 cm^{-1} for the [4-NH_2PyH][$BiCl_4$] crystal.

phase transitions at low temperature. In fact, the low temperature vibrational spectra indicate that the greatest changes are observed for the NH_2 and NH^+ groups.

4. Discussion

All the 4-aminopyridinium analogues (with the composition RMX_4) obtained so far appeared to be isomorphic in their high and low temperature phases. Below we compare the phase situation in these analogues:

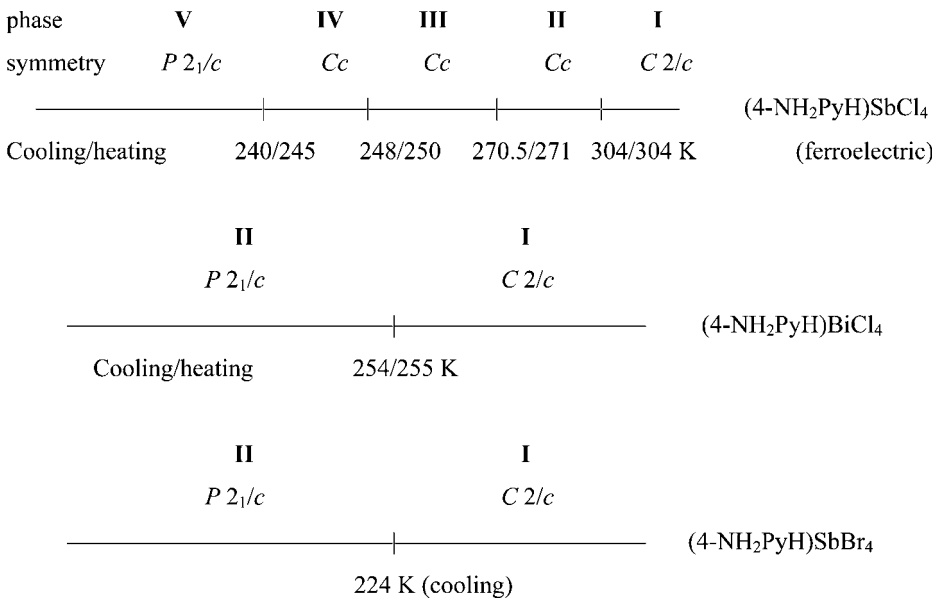

It is obvious that the highest temperature phases **I** in all crystals correspond to each other, whereas phase **V** of [4-NH_2PyH][$SbCl_4$] corresponds to phase **II** of the two remaining analogues, which is confirmed by the x-ray measurements. The appearance of the intermediate phases in the [4-NH_2PyH][$SbCl_4$] crystal dramatically changes its dielectric properties [15]. The phase transition $C2/c \rightarrow Cc$ leads to the ferroelectric order in this crystal. The mechanism of the ferroelectric phase transition at 270.5 K in [4-NH_2PyH][$SbCl_4$] was found to be rather complex. It was postulated that there are two molecular contributions to the phase transition. The first one appears to be an order–disorder type process due to the 120° reorientation of the organic cations (two-site model). The second mechanism is of a 'displacive' type. The latter contribution, connected with the displacement of the inorganic part with respect to the anionic sublattice, is dominant in the ferroelectric phase transition mechanism. In the case of [4-NH_2PyH][$SbBr_4$] [22] and [4-NH_2PyH][$BiCl_4$] crystals, which appear to be non-ferroelectric ones, only the 'order–disorder' type contribution from the 4-aminopyridinium cations is postulated.

It should be emphasized that dynamics of the 4-aminopyridinium cations over the high temperature phases seem to be common for all the above discussed crystals. In [4-NH_2PyH][$SbBr_4$] a favourable model for the cation disorder assumes the flipping of the cation by about 60° around the axis passing through the C7 atom (NH_2-C7) and perpendicular to the pyridinium ring (two-site model) [22]. In the [4-NH_2PyH][$BiCl_4$] crystal, the cations are able to perform simultaneously the 60° and 150° reorientation motion in the plane of the pyridinium ring, whereas for the [4-NH_2PyH][$SbCl_4$] crystal the 120° flipping motion is experimentally confirmed. The structural parameters of all RMX_4 type crystals such as the unit cell dimensions and the distances between the dipolar 4-aminopyridinium cations are comparable. This means that both the steric effects and sizes of cavities occupied by cations in the lattice are quite similar for these crystals. Despite the structural and dynamical similarities observed in RMX_4 crystals, nevertheless their dielectric properties are significantly different. This suggests that the dynamics of the organic moieties play a secondary role in the generation of ferroelectricity. It should be added, however, that the incommensurately modulated intermediate phase II in [4-NH_2PyH][$SbCl_4$] appears before reaching the ferroelectric phase (**III**) [28]. The motion of the cations over phase **II** is strongly restricted and the occupational modulation of these cations

takes place [29]. Thus, the role of the cation motion in the mechanism of ferroelectric transition is postulated to be minor.

A complete understanding of the phase transition mechanism in [4-NH_2PyH][$BiCl_4$] at 255 K requires an accurate analysis of the crystal structure for phases **I** and **II**. The main and the most drastic structural change appears to be the reorientation of the organic cations. While in phase **II** all organic moieties are completely ordered and occupy discrete positions, giving rather strong H-bonds, in the phase **I**, as a consequence of inorganic sublattice expansion (∼0.7% unit cell volume growth), there appears a weakening of H-bonds and growth of an amplitude of the thermal motion. Due to this, the 4-aminopyridinium moieties occupy larger volume. This leads to disorder of the organic cations. More than 80% of the cations occupy two positions (I and II) symmetrically related by the arising twofold axis. These positions seem to be completely overlapped (considering the accuracy is significantly affected by the thermal librations) except for the amino groups. Moreover, it should be added that considerable values of the temperature displacement factors of all atoms of the organic cations indicate a dynamic disorder rather than a statistical one for these moieties. The minor position III, occupied by less than 20% of the organic cations, is rotated by 150° with respect to position I or II. Distortion of the inorganic sublattice is not so drastic and results in averaging of the Bi–Cl distances related by arising elements of symmetry (see table 2). The only considerable change observed seems to be the elongation of inorganic fragments in the c direction (by ∼1.3%). As a result a weakening of the π–π type interactions between the neighbouring cations occurs. This facilitates the orientation of the cations in the plane perpendicular to the c-direction. Therefore, the phase transition is involved mainly by the disorder of the cation moieties, which arises from the inorganic sublattice expansion and results in the rearrangement of the hydrogen bonds.

A three-site model for [4-NH_2PyH][$BiCl_4$] seems to be confirmed by the calorimetric studies, since the transition entropy value ($\Delta S_{tr} = 10.1 \pm 1$ J mol^{-1} K^{-1}) resulting from DSC agrees well with the theoretical one ($R \ln 3 = 9.13$ J mol^{-1} K^{-1}). A sudden reduction of the mobility of the dipolar cations just below $T_{c(\mathbf{I}\rightarrow\mathbf{II})}$ is directly reflected in the dielectric characteristic ($\varepsilon(T)$) of the crystal. The proton magnetic resonance (T_1 and M_2) measurements disclosed an important role of the 4-aminopyridium reorientation in the dynamic properties of the [4-NH_2PyH][$BiCl_4$] crystal. A significant step-like decrease of the second moment (M_2) value exactly at 255 K is obvious evidence of the order–disorder mechanism of phase transition in the title crystal. It proves that the change in the motional state of the 4-aminopyridinium cations contributes mainly to the mechanism of the structural phase transition.

The vibrational studies on [4-NH_2PyH][$BiCl_4$] appeared to be interesting and important as well. It should be emphasized that the low temperature structural phase transitions exert a dramatic influence on the spectroscopic properties of the title crystal. The considerable temperature changes observed for the $\nu(NH^+)$, $\delta(NH^+)$ and γNH^+ modes suggest that the N-H$^+ \cdots$ Cl hydrogen bonds are also influenced by the phase transitions. Enormous changes with temperature of the band positions and their FWHM for numerous bands assigned to the vibrations of the NH_2 group and C–H bonds at 250 K clearly indicate that the 4-aminopyridinium moieties play an important role in the phase transition mechanism of the [4-NH_2PyH][$BiCl_4$] crystal.

5. Conclusions

(i) The [4-NH_2PyH][$BiCl_4$] crystal appeared to be isomorphic (centrosymmetric, monoclinic space group, $C2/c$) with [4-NH_2PyH][$SbBr_4$] and the recently discovered incommensurately modulated ferroelectric [4-NH_2PyH][$SbCl_4$] crystal at room temperature.

(ii) The [4-NH_2PyH][$BiCl_4$] crystal consists of chains of polymeric $(BiCl_4^-)_\infty$ anions forming a tunnel-like structure. The chains are joined together by the 4-aminopyridinium cations, whose N–H bonds form hydrogen bonds to the chlorine atoms of the chains.
(iii) The 4-aminopyridinium cations are found to be highly disordered in phase **I**, being distributed over three positions with various occupancy factors.
(iv) [4-NH_2PyH][$BiCl_4$] undergoes a perfectly reversible discontinuous phase transition at 254/255 K (cooling–heating) with an order–disorder mechanism.
(v) The second moment of ^{1}H NMR and the infrared measurements clearly confirmed a contribution of the 4-aminopyridinium cation motion to the phase transition mechanism at 255 K.

Acknowledgment

This work was supported by the Polish State Committee for Scientific Research (project register 3 T09A 049 26).

References

[1] Jakubas R and Sobczyk L 1990 *Phase Transit.* **20** 163
[2] Sobczyk L, Jakubas R and Zaleski J 1997 *Pol. J. Chem.* **71** 265 and references cited therein
[3] Ishihara H, Yamada K, Okuda T and Weiss A 1993 *Bull. Chem. Soc. Japan* **66** 380
[4] Gesi K, Iwata M and Ishibashi Y 1995 *J. Phys. Soc. Japan* **64** 2650
[5] Kuok M H, Ng S G, Tan L S, Rang Z L, Iwata M and Ishibashi Y 1998 *Solid State Commun.* **108** 159
[6] Jakubas R, Krzewska U, Bator G and Sobczyk L 1988 *Ferroelectrics* **77** 129
[7] Zaleski J and Pietraszko A 1996 *Acta Crystallogr.* B **52** 287
[8] Zaleski J, Pawlaczyk Cz, Jakubas R and Unruh H-G 2000 *J. Phys.: Condens. Matter* **12** 7509
[9] Bator G, Jakubas R, Zaleski J and Mróz J 2000 *J. Appl. Phys.* **88** 1015
[10] Bujak M and Zaleski J 2001 *Cryst. Eng.* **4** 241
[11] Lefebvre J, Carpentier P and Jakubas R 1995 *Acta Crystallogr.* B **51** 167
[12] Pavel M, Fouskova A, Jakubas R and Miniewicz A 1993 *Ferroelectrics* **146** 37
[13] Jóźków J, Jakubas R, Bator G and Pietraszko A 2001 *J. Chem. Phys.* **114** 7239
[14] Jakubas R, Piecha A, Pietraszko A and Bator G 2005 *Phys. Rev.* B **72** 104107
[15] Jakubas R, Bator G and Ciunik Z 2003 *Phys. Rev.* B **64** 024103
[16] Przesławski J, Kosturek B and Jakubas R 2003 *J. Phys.: Condens. Matter* **15** L643
[17] Bator G and Jakubas R 2003 *J. Phys. Soc. Japan* **72** 2369
[18] Oxford Diffraction 2003 CrysAlis CCD and CrysAlais RED *Oxford Diffraction Poland,* Wrocław, Poland
[19] Sheldrick G M 1997 *SHELXL97, Program for Solution of the Crystal Structures* University of Goettingen
[20] Tolédano P and Tolédano J-C 1982 *Phys. Rev.* B **25** 1946
[21] Hashimoto M, Hashimoto S, Terao H, Kuma M, Niki H and Ino H 2000 *Z. Naturf.* a **55** 167
[22] Hashimoto M, Terao H, Fuess H, Svoboda I and Ehrenberg H 2003 *Bull. Chem. Soc. Japan* **76** 749
[23] Medycki W, Hołderna-Natkaniec K, Świergiel J and Jakubas R 2004 *Solid State NMR* **25** 129
[24] Akyuz S 1999 *J. Mol. Struct.* **482** 171
[25] Buyukmurat Y and Akyuz S 2003 *J. Mol. Struct.* **651** 533
[26] Ivanova B B and Mayer-Figge H 2005 *J. Coord. Chem.* **58** 653
[27] Ivanova B B, Arnaudov M G and Mayer-Figge H 2005 *Polyhedron* **24** 1624
[28] Przesławski J, Kosturek B and Jakubas R 2003 *J. Phys.: Condens. Matter* **15** L643
[29] Pietraszko A, Czopnik R and Jakubas R 2004 *Acta Crystallogr.* A **60** S257